

# COMPARISON OF OVERLAPPING AND SEPARATE DOMAIN COUPLING METHODS

**T. P. Grunloh and A. Manera**

Department of Nuclear Engineering and Radiological Sciences, University of Michigan-Ann Arbor,  
2355 Bonisteel Blvd., Ann Arbor, MI 48109, USA  
grunloh@umich.edu, manera@umich.edu

## ABSTRACT

A coupling infrastructure code, *Janus*, has been developed at the University of Michigan, providing methods for the online data transfer between the commercial CFD code STAR-CCM+ and the best-estimate thermal hydraulic system code TRACE, developed by the US NRC. Coupling between these two software packages is motivated by the desire to extend the range of applicability of TRACE to scenarios in which local momentum transfer and three-dimensional effects are important, such as circulation through an open region. The intra-fluid shear forces neglected by TRACE equations of motion are readily calculated in CFD solutions. Consequently, the coupling methods used in this study are built around correcting TRACE solutions based on data from a corresponding STAR-CCM+ solution.

Two coupling strategies are discussed, one based on an overlapping domain approach and a second based on separate domains. These coupling methods have been applied to the simulation of open and closed loops in both steady state and transient operation. The objective of this study is to examine the effect of each coupling method on convergence, consistency, and numerical stability.

As expected, the results produced by the two methods were found to be identical, and consistent with the standalone TRACE solution in both steady state and transient cases. However, the overlapping domain method was found to achieve convergence at larger integration time steps than the separate domain approach and exhibited superior convergence and numerical stability characteristics in both steady state and transient scenarios.

## KEYWORDS

coupling, separate, overlapping, TRACE, CFD

## 1. INTRODUCTION

### 1.1. Motivation

The capabilities of best-estimate system codes such as TRACE [1], RELAP5 [2], CATHARE [3], and ATHLET [4] to simulate large networks of interconnected Nuclear Power Plant (NPP) components has been well established and documented in an ample body of literature. However, in some scenarios, the assumptions used in these codes to simplify the set of flow conservation equations become invalid, especially when three-dimensional effects play an important role in the transient scenario to be analyzed. Specifically, best-estimate system codes are unable to correctly capture circulating flow patterns in large open regions which are, for example, important in investigation of the behavior of passive safety systems and flow mixing in the downcomer and lower plenum of the reactor pressure vessel (RPV).

Recent years have shown significant maturation of Computational Fluid Dynamic (CFD) methods towards the efficient simulation of single phase flow in complex geometries relevant to nuclear

engineering [5] [6] [7]. Additionally, the enduring trend of increased availability of computational resources continues to add larger models to the class of tractable problems. Therefore, coupling of CFD codes with best-estimate thermal-hydraulic system codes has become a worthwhile endeavor, particularly in view of current industry trends characterized by power uprates, with the consequent reduction of safety margins, which require a compensating increase in the fidelity of computational models.

Several efforts focused on the coupling between CFD and system codes have been reported in the literature. Primarily, two spatial decomposition approaches are described, referred to as separate domain and overlapping domain approaches. In the former, the system to be modeled is divided into two domains, one simulated using the system code and the other computed within the CFD code, with information exchange at the domain interfaces. In the overlapping domain approach, the entire system is computed within the system code, with selected regions also simulated within the CFD code. The first coupling efforts reported in the literature were from Aumiller and co-workers [8] and Gibeling and Mahaffy [9]; both works were based on separate domain approach. In the last years several additional efforts have been based on the same approach [10] [11] [12] [13] [14]. In [8] [11] [12] semi-implicit numerical coupling schemes are also described, aimed at relaxing the requirements on the integration time steps posed by explicit time-stepping methods.

Overlapping domain approaches are employed in the coupling schemes described in Refs. [15] to [16]. In the coupling developed by Fanning and Thomas [15], the CFD solution is used to correct the energy equation and the gravitational pressure term computed by the system code. Jeltsov and coauthors [17] use the CFD solution only to correct the system code energy equation through the implementation of a “virtual heater”. In the coupling between the CFD code TRIO-U and the system code CATHARE, the CFD solution is used to correct both momentum and enthalpy equations [16] using controls. In Refs. [17] and [18] a simple correction of the system code momentum equation is described based on the overall pressure drop computed by the CFD code, however it is unclear how inertial and non-inertial pressure drops are treated when combined with an explicit numerical coupling scheme such as the one used in these references.

Comparisons among coupled CFD/system-codes based on overlapping and separate domain approaches have been reported in the literature [19] [20]. However, due to the fact that different coupled codes were used (RELAP5/STAR-CCM+, ATHLET/ANSYS-CFX, CATHARE/TRIO-U), these comparisons cannot be used to draw generalized conclusions on the performance of a given coupling scheme versus another.

The present paper is focused on the systematic analysis of separate and overlapping domain coupling strategies, with special focus on the coupling of the momentum equation and the treatment of inertial and non-inertial pressure drop terms. Both separate and overlapping domain methodologies have been implemented using the US NRC system thermal hydraulic code TRACE and the commercial CFD code STAR-CCM+. After laying down the theoretical basis for the proposed coupling infrastructure, the performance of the two domain decomposition methodologies are characterized through a systematic analysis of open and closed loop flow systems. The two coupling methodologies are described in section 2 and a comparison between the two methodologies is reported in sections 3 and 4.

## **2. COUPLING METHODOLOGIES**

### **2.1. Separate Domain Approach**

Separate domain coupling is realized through the transfer of data at boundaries between distinct regions, each modeled either with the system code or with the CFD code. A schematic of the separate domain coupling strategy employed in this study is shown in Figure 1. A separate domain interface can connect a TRACE BREAK (pressure boundary condition) component to a STAR-CCM+ inlet boundary (Figure 1

left), or a TRACE FILL (mass flow or velocity inlet) component to a STAR-CCM+ pressure outlet boundary (Figure 1 right). In the case of the former, the pressure calculated at the inlet of the CFD region is passed to the cell center of the BREAK component and the flow rate in the BREAK is passed to the CFD inlet. In the case of the latter, the pressure at the center of the cell nearest the interface is passed to the CFD outlet boundary while the flow rate through the CFD outlet is passed to the FILL component.

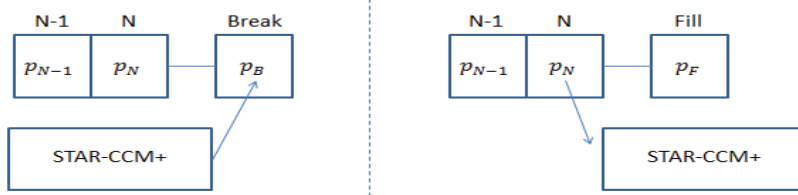


**Figure 1. Schematic diagram for implementation of surface interfaces for data exchange between boundaries of TRACE and STAR-CCM+**

The coupling method described here does not pass data exactly at the interface and makes no attempt to correct this through interpolation or any other method. However, the error at each interface is limited to the pressure drop across one half of a cell. Since this distance is generally small with respect to the global geometry, the error is negligible. The real benefit of separate domain coupling lies in its simplicity. Neglecting the error incurred from the first order coupling method, the pressure drop imposed on TRACE with separate domain coupling in both transient and steady state is given by Equation 1:

$$\Delta P_{sep} = \Delta P_{CFD} \quad 1$$

## 2.2. Overlapping Domain Approach

In the overlapping domain coupling paradigm, the entire flow domain is simulated with the system code, while only a portion of the domain is further simulated with the CFD code. The codes are then volumetrically coupled in the overlapping region. In this case, TRACE simulates the entire flow system, while STAR-CCM+ is constrained to a smaller portion of the flow domain. The TRACE solution is then corrected internally based on data from STAR-CCM+ in order to make the system code solution more “CFD-like” motivated by the assumption that, in appropriate regions, the CFD solution will be more accurate than the system code solution.

A simplified version of the one-dimensional equation of motion implemented in TRACE is given in Eq. 2.  $V_{j+1/2}^{n+1}$  refers to the new time velocity at the edge between cells  $j$  and  $j + 1$  while  $\langle \rho \rangle_{j+1/2}^n$  refers to the average liquid density,  $\Delta x$  is the distance between centers of neighboring cells, and is a  $K_{j+1/2}^n$  loss coefficient calculated through correlation.

$$\frac{V_{j+1/2}^{n+1} - V_{j+1/2}^n}{\Delta t} + V_{j+1/2}^n \frac{\partial V^{n+1}}{\partial x} \Big|_{j+1/2} = - \frac{1}{\langle \rho \rangle_{j+1/2}^n} \frac{P_{j+1}^{n+1} - P_j^{n+1}}{\Delta x} - K_{j+1/2}^n [2V_{j+1/2}^{n+1} - V_{j+1/2}^n] |V_{j+1/2}^n| \quad 2$$

Comparison to the Navier-Stokes momentum balance equations shows that the divergence of the stress tensor  $\mathbf{T}$  in a system code like TRACE is modeled as proportional to the square of a velocity. The constant of proportionality is calculated from the Churchill correlation of the Fanning friction factor [1].

$$-\frac{\nabla \cdot \mathbf{T}}{\rho} \approx KV^2 = \frac{2f_F}{D_h} V^2 \quad 3$$

Based on this analysis, a CFD based friction factor can be calculated from the definition of the Fanning friction factor [21], as shown in Eq. 4, similar to the treatment used by other researchers [22].

$$f_{CFD} = \frac{1}{2} \frac{D_h}{\rho_{TRC} (V_{j+1/2}^n)^2} \frac{\Delta P_{CFD}}{L_{LP}} \quad 4$$

The CFD friction factor defined in Eq. 4 is computed based on the global pressure drop across the CFD component,  $\Delta P_{CFD}$ . Because this pressure drop includes the acceleration pressure drop calculated in CFD, the associated term is ignored in the TRACE momentum equation, but only for the coupled component. Division by a lumped parameter (LP) length scale  $L_{LP}$  creates an average pressure gradient. The length scale  $L_{LP}$  is the length of the overlapped component as defined in TRACE and is automatically retrieved from the TRACE input data by the coupling. The average pressure gradient is then normalized by the hydraulic diameter ( $D_h$ ) and the local TRACE values for density ( $\rho_{TRC}$ ) and old time step velocity ( $V_{j+1/2}^n$ ). This coupling methodology allows the system code to solve the mass and momentum balance equations for the entire system and prevent mass conservation inconsistencies that can be problematic for closed loop simulations [12].

Combining Equations 2, 3, and 4 as well as assuming steady state and skipping the acceleration term (only for coupled components where this term is corrected by CFD), the pressure drop across the  $j + 1/2$  face is calculated as shown in Eq. 5. Thus, the pressure drop across an edge is simply the total CFD pressure drop scaled down to the correct length for edge  $j + 1/2$ .

$$\Delta P_{j+1/2} = -\text{sign}\left(V_{j+\frac{1}{2}}\right) \Delta P_{CFD} \left(\frac{\Delta x}{L_{LP}}\right) \quad 5$$

However, in a transient simulation, the presence of the inertial term can lead to substantial differences between the pressure drop in STAR-CCM+ and TRACE as shown in Eq. 6, if adequate care is not taken in the implementation of the coupling scheme.

$$\Delta P_{j+1/2} = -\rho \Delta x \frac{V_{j+\frac{1}{2}}^{n+1} - V_{j+\frac{1}{2}}^n}{\Delta t} - \Delta x \frac{1}{\left(V_{j+\frac{1}{2}}^n\right)^2} \frac{\Delta P_{CFD}^n}{L_{LP}} \left(2V_{j+\frac{1}{2}}^{n+1} - V_{j+\frac{1}{2}}^n\right) \left|V_{j+\frac{1}{2}}^n\right| \quad 6$$

Consistency between CFD and system code is achieved by computing a non-inertial pressure gradient based friction factor. Starting from the Navier-Stokes equations, the pressure gradient can be partitioned into three distinct terms as shown in in Eq. 7. The first term on the right results from unsteady velocities, and will be referred to as the inertial pressure contribution. The second term on the right results from acceleration due to velocity gradients and is referred to as the acceleration pressure gradient. Finally, the frictional pressure gradient resulting from viscous dissipation is the third term on the right. In cases of turbulent flow, consider  $\mathbf{v}$  to be the Reynolds averaged velocity and for  $\bar{\mathbf{T}}$  to include Reynolds stresses.

$$\nabla p = -\rho \frac{\partial \mathbf{v}}{\partial t} - \rho \mathbf{v} \cdot \nabla \mathbf{v} + \nabla \cdot \bar{\mathbf{T}} \quad 7$$

In an operator-splitting explicit numerical coupling scheme, it is not straightforward to correct for the inertial pressure term. However, given that, in this study, the CFD solution is computed for incompressible single-phase domains, we can safely assume that the difference between the inertial pressure drops as computed by CFD and the system code is negligible. Therefore, only the non-inertial pressure drop terms (acceleration and friction) need to be corrected. In order to cast the CFD solution into data usable for TRACE, a volume averaged non-inertial (NI) pressure gradient is defined.

At this point, it is convenient to focus on assumptions specific to 1D pipe type components. Such test cases provide excellent grounds for establishing proof-of-principle calculations. A more general interface applicable to 3D geometries, such as open regions with recirculation, based on the same foregoing principles has been developed and will be presented in a future paper.

In order to condense the pressure gradient vector field into a scalar, the integrand of Eq. 8 is dotted with a *flow path vector*  $\mathbf{n}_{fp}$ . Such a vector is needed because the 1D definition of components in system thermal-hydraulic (STH) codes entails information about flow direction not otherwise available to CFD. This vector field is physically interpreted as the direction of the mean flow at each cross section and can be readily calculated from geometric data available to the STH code for 1D components.

$$\langle \nabla p \cdot \mathbf{n}_{fp} \rangle_{NI} = \langle (\nabla \cdot \bar{\mathbf{T}}) \cdot \mathbf{n}_{fp} \rangle - \rho \langle \mathbf{v} \cdot (\mathbf{n}_{fp} \cdot \nabla \mathbf{v}) \rangle \quad 8$$

The volume integral of the divergence of the stress tensor can be rewritten as a surface integral using the divergence theorem. This step is taken to avoid the calculation of second derivatives of the velocity field, which are not natively available through most CFD codes.

$$\langle (\nabla \cdot \bar{\mathbf{T}}) \cdot \mathbf{n}_{fp} \rangle = \frac{1}{Vol} \iiint (\nabla \cdot \bar{\mathbf{T}}) \cdot \mathbf{n}_{fp} dV = \frac{1}{Vol} \oint [(\bar{\mathbf{T}} \cdot \mathbf{n}_{fp}) \cdot \mathbf{n}] dS - \frac{1}{Vol} \iiint \bar{\mathbf{T}} : \nabla \mathbf{n}_{fp} dV \quad 9$$

The geometry in use for the specific test cases in hand lies entirely along one coordinate ( $\mathbf{n}_{fp} = \hat{\mathbf{e}}_x$ ), allowing for a simpler expression for the friction factor in Eq 10.

$$f_{CFD} = \frac{1}{2} \frac{D_h}{\rho_{TRC} (V_{j+1/2}^n)^2} \left[ \frac{1}{Vol} \oint (\bar{\mathbf{T}} \cdot \mathbf{n}) \cdot \hat{\mathbf{e}}_x dS - \frac{1}{Vol} \iiint \rho (\mathbf{v} \cdot \nabla \mathbf{v}) \cdot \hat{\mathbf{e}}_x dV \right] \quad 10$$

Specifically, this formulation for the friction factor is based on the difference between *surface averaged* pressures between the inlet and outlet of the STAR-CCM+ region, excluding the contribution of the inertial term to the pressure gradient. Since TRACE actually calculates cell *volume averaged* pressures, this leads to some geometrical error, approximately equal to the ratio of the length of one STH cell to the length of the entire component (either 1/18 or 1/20 for the simulations in this paper).

The friction factor of Eq. 10 was calculated by only considering the non-inertial components of the pressure gradient. An obvious alternative computation method, shown in Eq. 11, is to simply subtract the inertial portion of the pressure gradient from the total pressure gradient, still relying on the assumption that the difference between the inertial pressure drop term as computed by TRACE and STAR-CCM+ is negligible.

$$f_{CFD}^{alt} = \frac{1}{2} \frac{D_h}{\rho_{TRC} (V_{j+1/2}^n)^2} \left[ \frac{\Delta P_{CFD}^{n+1}}{L_{LP}} - \frac{1}{\Delta t} \left( \iiint \rho \mathbf{v}^{n+1} \cdot \mathbf{n}_{fp} dV - \iiint \rho \mathbf{v}^n \cdot \mathbf{n}_{fp} dV \right) \right] \quad 11$$

The alternative non-inertial friction factor of Eq 11 has been implemented and found to produce identical results as Eq. 10 for the 1D test cases in this paper. As a point of clarification, the reader is reminded that Eqs. 10 and 11 are only applicable to pipe geometries in which is  $\mathbf{n}_{fp}$  easily defined. The extension to cases in which the definition of  $\mathbf{n}_{fp}$  is not straightforward will be discussed in a companion paper.

### 3. RESULTS

#### 3.1. Open Loop Test Case Description

A case previously explored by Bertolotto [23] utilizes a 3 meter pipe with a radius of 0.025 meters. In the coupled cases, the first 2 meters of the pipe are simulated with TRACE while the remaining meter is coupled to STAR-CCM+ through either separate domains (Figure 2 left) or overlapping domain (Figure 2 right) methods. The flow in the pipe is initially stagnant and at a constant pressure of  $p_{init} = 10 \text{ bar}$ . At time  $t = 5.0 \text{ s}$ , the pressure at the outlet is abruptly lowered to  $p_{out}(t \geq 5.0 \text{ s}) = 9.9 \text{ bar}$ . The resulting transient is carried out for a period of 10 seconds.

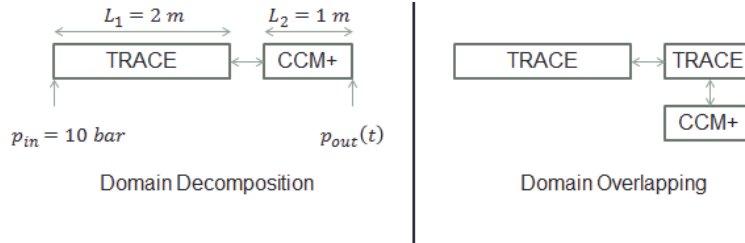


Figure 2. Schematic diagrams of the abrupt pressure drop test case coupling configurations.

#### 3.2. Open Loop Test Case Analytic Treatment

One benefit of the test case described in Figure 2 is that it lends itself quite well to analytic treatment. Immediately after  $t = 5.0 \text{ s}$ , the total pressure drop across the pipe is held constant at  $\Delta P = 10 \text{ kPa}$ . Because the pipe is constant in cross section and without flow changes, the only contributions to the pressure drop are the inertial and frictional terms of the momentum equation. Utilizing the Fanning friction factor to model the frictional terms yields Eq. 12 as the governing equation of the system, where  $L = L_1 + L_2$  is the total length of the system as shown in Figure 2.

$$\Delta P = 10 \text{ kPa} = \Delta P_f + \Delta P_I = 2f_F \frac{L}{D} \rho V^2 + L\rho \frac{\partial V}{\partial t} \quad 12$$

For small times, the frictional term is dominated by the inertial term and the initial velocity gradient can be estimated with Eq. 13.

$$\left. \frac{\partial V}{\partial t} \right|_{t=5s} = \frac{\Delta P}{\rho L} \quad 13$$

It is useful to apply Eq. 13 to the first iterative cycle of an explicit separate domain coupled calculation. Before any iteration occurs, the mass flow rate of STAR-CCM+ is set to zero and the pressure everywhere is uniform. The pressure of the outlet is then lowered abruptly. At this point the mass flow rate is still everywhere zero. However, the TRACE part of the pipe is at the inlet pressure while the STAR-CCM+ section is at the outlet pressure. The STAR-CCM+ outlet pressure is then translated to the outlet of the TRACE section. TRACE then calculates the new velocity with Eq 14.

$$\left. \frac{\partial V}{\partial t} \right|_{t=5s} = \frac{\Delta P}{\rho L_1} > \frac{\Delta P}{\rho L} \quad 14$$

Thus, it can be observed that an explicit separate domain coupling will overestimate the velocity at the first timestep by a factor of  $L/L_1$ , which is 1.5 in the case of the geometry in Figure 2. Because the entire length of the component is available to TRACE in the case of overlapping domain coupling, this effect does not occur if overlapping domain is used in place of separate domain coupling.

### 3.3. Open Loop Abrupt Pressure Drop

The time-trace of the mass flow-rates resulting from the abrupt pressure drop are shown in Figure 3 for both coupling methods, and different integration time steps, ranging between 0.01 and 1 s. Additionally, the data calculated by Bertolotto with semi-implicit separate-domain coupling using CFX/TRCACE are plotted as a reference. Domain overlapping cases appear to converge for quite large timesteps, with even the largest timesteps producing qualitatively accurate results. The first step overshoot of the separate domain approach predicted by Eq 14 is especially apparent for the “ $dt = 1.0$ ” case (Figure 3 bottom). Close inspection shows that the “ $dt = 0.025$ ” case follows the same slope initially, as is expected. The overshoot results in the mass flow rate being under predicted in the  $t \in [6s, 8s]$  range for the cases with  $dt < 1.0s$ . From Figure 3, it can be estimated that the domain overlapping case converges with a  $dt = 0.1 s$  while the domain decomposition method requires  $dt = 0.0025s$ . Thus, a significant savings in terms of integration time step, and thus computational resources requirements, is realized.

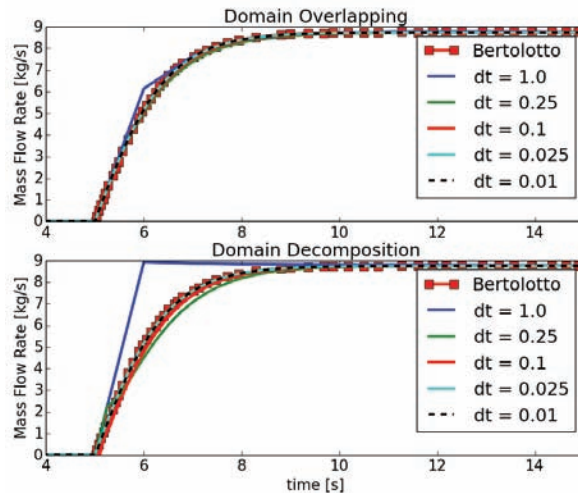


Figure 3. Mass flow rates through the open loop as a function of time for both coupling methods.

### 3.4. Pump Driven Closed Loop Test Case Description

The loop analyzed in this section, as shown in Figure 4, consists of three pipe sections, a pump, and a pressure setpoint to prevent runaway pressures from building up within the loop. The pump is driven by a custom pump head curve designed to produce the desired mass flow rates.

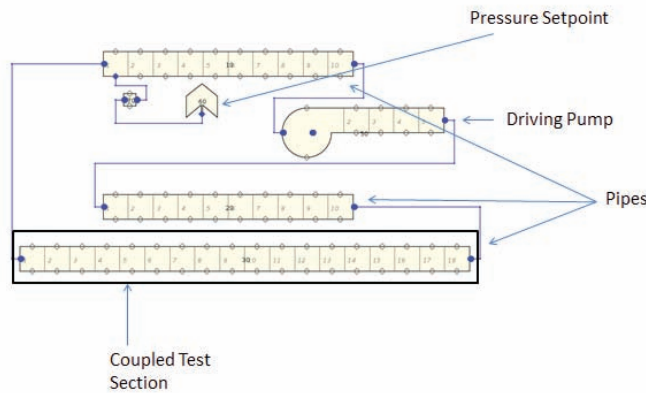


Figure 4. TRACE model of closed, pump driven loop.

The test section modeled with CFD is highlighted in Figure 4 and consists of a 1.8 m long circular pipe with a diameter of 0.1 m. For the overlapping domain approach, this section is modeled also within TRACE using 18 cells of equal length. The analogous STAR-CCM+ component is a circular tube of the same dimensions as the TRACE pipe and is composed of approximately 23000 cells. System codes like TRACE are based on the assumptions that the flow is fully developed. To have a fully consistent formulation between CFD and system code, a fully developed velocity profile should be imposed at the interface between the TRACE and CFD domains. However, for the current test case, flat inlet velocity profiles with default turbulence parameters are imposed at the inlet of the CFD domain. This is sufficient to test the coupling methodology and allows for additional basis for testing, since a given mass flow-rate produces a higher pressure drop when compared to standalone TRACE simulations. This distinction between STAR-CCM+ and TRACE results allows for visual confirmation of the coupled simulations through the resulting mass flow rate and pressure drop profiles.

### 3.5. Interfacing

The overlapping domain technique is applied through one volume interface connecting the test section in the complete TRACE model to the CFD model of the component as shown in Figure 5. The left side of the STAR-CCM+ pipe is a mass flow inlet held at the same mass flow rate as the TRACE pipe. At each timestep, the average pressure gradient (denoted by  $\langle \partial p / \partial x \rangle$  in Figure 5) is passed from CFD to TRACE through a friction factor calculated by Eq. 10. The right side of the CFD model is held at a constant pressure, while the right and left sides of the TRACE model are connected to pipes as shown in Figure 4.

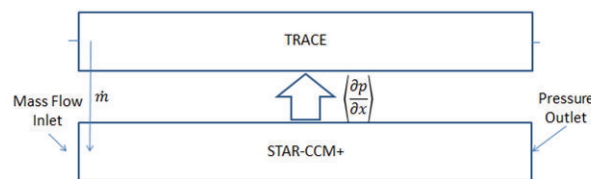


Figure 5. Schematic diagram of overlapping domain coupling technique.

Separate domain coupling techniques are applied to the closed loop by removing the test section (highlighted in Figure 4) from the TRACE model, using STAR-CCM+ for this region instead, and communicating pressure and mass flow data via two interfaces at either end of the CFD component as shown in Figure 6. The left side of the STAR-CCM+ component is a mass flow inlet receiving an interfacial mass flow rate ( $\dot{m}_i$ ) from a BREAK (pressure boundary condition) component in TRACE and, in turn, providing a pressure ( $p_i$ ). The right side of the CFD component is a pressure boundary that receives a pressure ( $p_i$ ) from a FILL component (mass flow rate boundary) in TRACE and, in turn, provides a mass flow rate ( $\dot{m}_i$ ) to TRACE.



Figure 6. Schematic diagram of separate domain coupling technique showing the interfacial quantities being exchanged.

### 3.6. Steady State

Steady state mass flow rate results from the coupled cases are compared to the uncoupled TRACE standalone solution in Figure 7. Even though, due to the use of a uniform velocity profile at the inlet of the CFD domain in the coupled simulations, an extra friction loss is incurred by the developing flow in the CFD pipe section, the effect on the total mass flow rate through the loop is negligible, as expected, and the curves closely overlap.

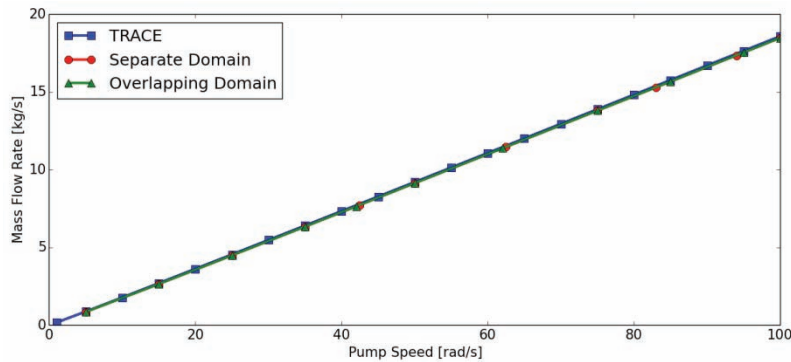


Figure 7. Steady state mass flow rates achieved via both coupling methodologies as compared to those calculated via TRACE standalone simulation.

#### 3.6.1. Convergence Characteristics - Separate Domain Coupling

In Figure 8, the data passed from TRACE to STAR-CCM+ at each iteration is plotted for a test case (steady-state) with a pump impeller rotation rate of 50  $rad/s$  (Figure 8 left) and 5  $rad/s$  (Figure 8 right) using several under relaxation factors (0.3, 0.6, and 1.0) applied to the mass flow rate output by TRACE. Based on this data, under relaxation appears unnecessary as lower relaxation factors lead to more iterations required for convergence.

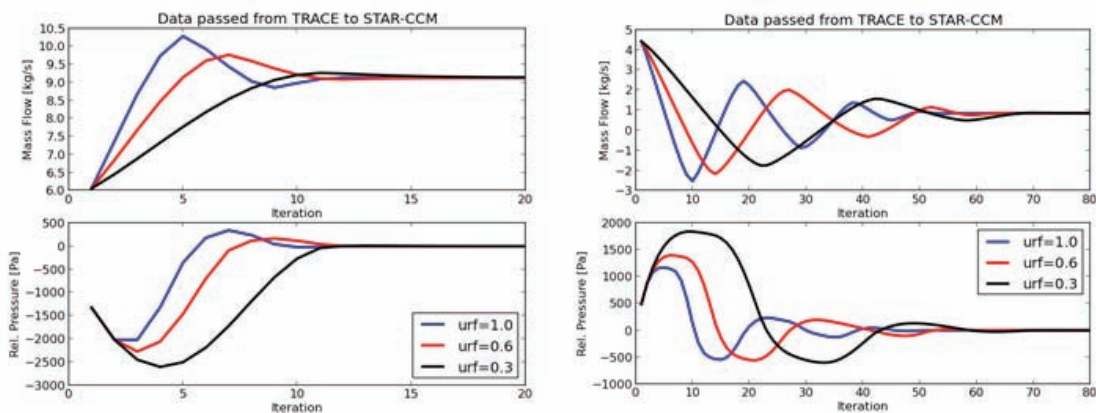
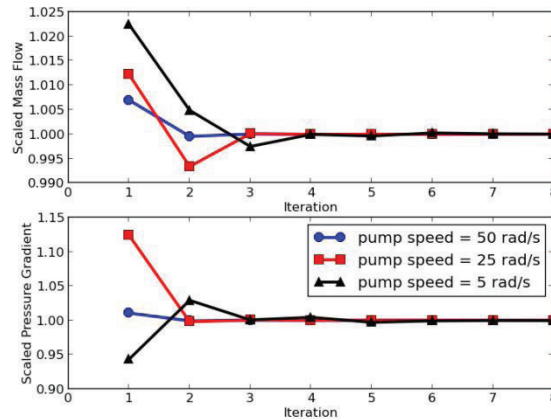


Figure 8. Convergence data collected for steady state closed loop separate domain case for several different under relaxation factors. A pump speed of 50  $rad/s$  is used for the data on the left while a speed of 5  $rad/s$  is used for data on the right.

#### 3.6.2. Convergence Characteristics - Overlapping Domain Coupling

Based on results in Figure 8, no under relaxation was applied for the overlapping domain case. Data passed through the interface at each iteration are shown in Figure 9 for three different pump speeds.

Convergence is achieved in five or fewer iterations for all speeds considered. It can also be noted that convergence is achieved with a much smaller number of iterations when compared to the separate domain results presented in Figure 8.



**Figure 9. Convergence behavior of the closed loop coupled with overlapping domain techniques for selected pump speeds.**

### 3.7. Transient

Currently, only explicit coupling has been implemented in the Janus infrastructure for transient simulations. Individually, STAR-CCM+ uses the “Implicit Unsteady” temporal solver, while TRACE uses the Stability Enhancing Two Step (SETS) solver by default [1] [24]. The coupling scheme used for the present analysis entails TRACE first calculating a timestep from time  $t^n$  to  $t^{n+1}$ , then passing the new time data to STAR-CCM+ which then takes the same time step. The inverse of this was also tested and found to have similar accuracy.

For a transient test of the closed loop, the pump impeller rotation rate was pulsed according to the function in Equation 15, designed to be smooth up to at least the first derivative, and the system response was measured through the mass flow rate through the loop and the pressure drop across the coupled test section (highlighted in Figure 4).

$$\Omega(t) = \begin{cases} 50.0 \frac{rad}{s}, & t \leq 100.0s \\ 50.0 \left[ 1 + \sin^4 \left( \frac{t - 100.0s}{10.0s} \pi \right) \right] \frac{rad}{s}, & 100.0s < t < 110.0s \\ 50.0 \frac{rad}{s}, & t \geq 110.0s \end{cases} \quad 15$$

#### 3.7.1. Separate Domain

Response functions for the mass flow-rate and pressure drop across the test section are shown in Figure 10 alongside temporal convergence data. As expected, the mass flow rate appears to converge to a function resembling the pump impeller rotation rate, while the pressure drop converges to a function resembling the time derivative of the mass flow rate. An unphysical pressure peak is present for very large timesteps around  $dt \sim 1.0s$ .

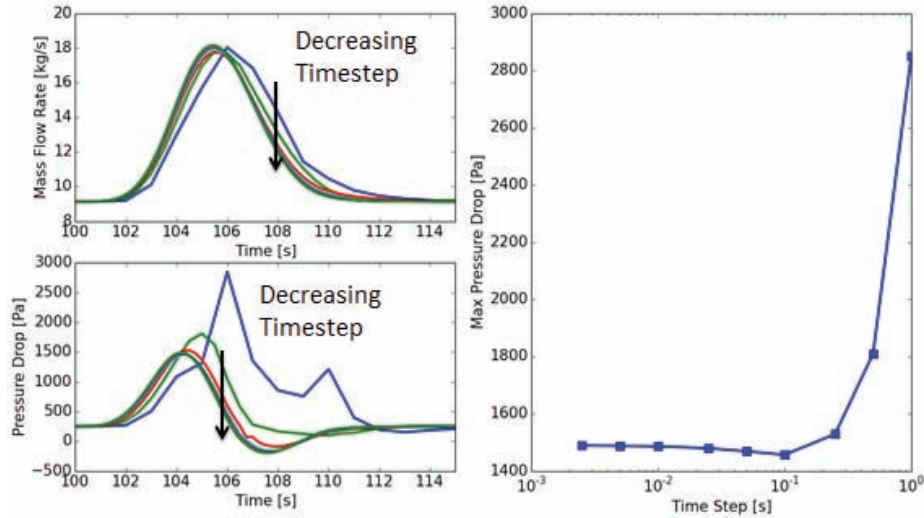


**Figure 10. Transient response functions and temporal convergence data for separate domain coupling pump driven close loop test case**

The maximum pressure drop is plotted on the right of Figure 10 for each time step tested, giving an indication of the temporal convergence of the pressure response function. Significant error reduction is evident in the region  $dt \in [10^{-1}s, 10^0s]$ , while the reduction drops off markedly for  $dt < 10^{-1}s$ .

### 3.7.2. Overlapping Domain

The transient pump speed of Equation 15 was also applied to the overlapping domain coupled model with transient response functions and convergence data shown in Figure 11.

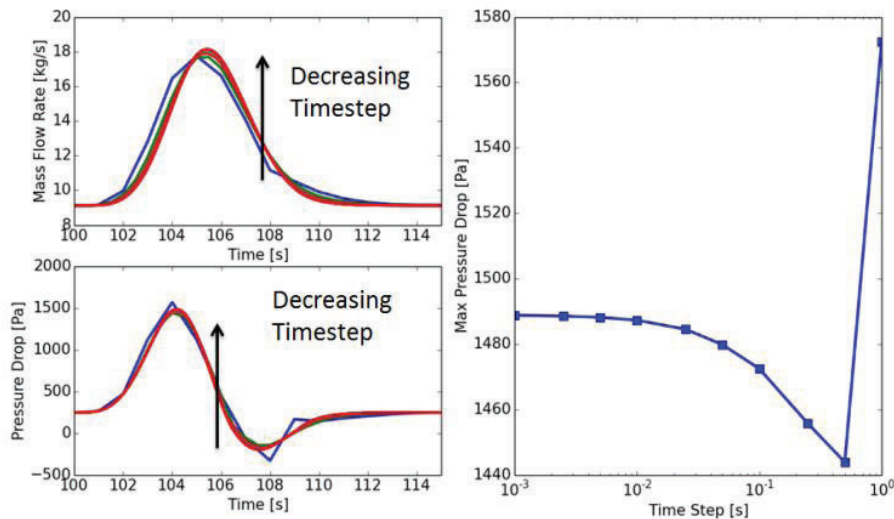


**Figure 11. Mass flow rate and pressure drop response functions alongside temporal convergence data for the overlapping domain pump driven close loop transient test case.**

The response functions for all time steps tested show qualitatively similar behavior. Larger time steps appear to primarily shift the curves to the left, rather than significantly altering the character of the function. Temporal convergence appears to be realized near  $dt = 0.025 s$ .

## 4. DISCUSSION

The data of Figure 8 and Figure 9 show favorable steady state stability properties of overlapping domain coupling methods. While some separate domain cases required up to 80 iterations to converge, all overlapping domain cases tested required only 5-8 iterations. Under-relaxation was not found to aid convergence for the separate domain cases. The improved performance of the overlapping domain method is a direct result of maintaining system wide pressure balances within the system code, as shown in section 3.2.

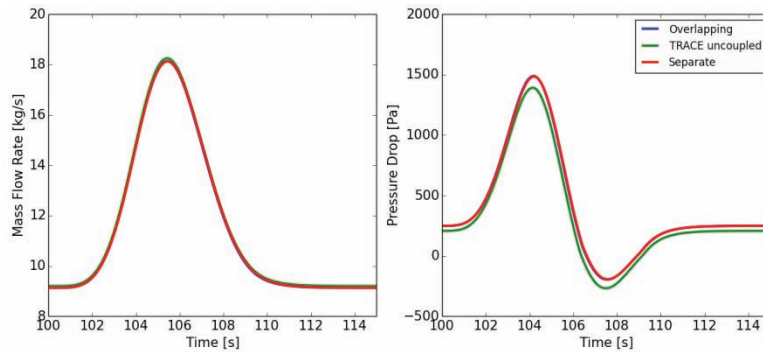


**Figure 12. Converged mass flow rate and pressure drop response functions for the closed loop as calculated with 3 methods. method ( $dt = 2.5\text{ ms}$ ).**

Mass flow rate and pressure drop profiles throughout transient simulations are shown in Figure 12 for both coupling methods and TRACE standalone, showing that the coupled simulations produce identical results. The pressure drop functions for the coupled cases are slightly higher due to the flat inlet profiles imposed on the CFD pipe, providing confirmation that the coupling is implemented correctly in that it corrects the TRACE results to match the CFD results.

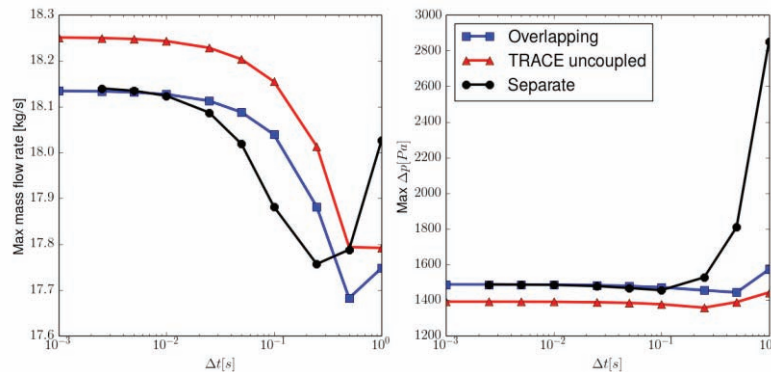


**Figure 13. Plots of maximum values of mass flow rate and pressure drop across the coupled section against the timestep used for each transient case tested.**

The maximum values of mass flow rate and pressure drop are plotted against time step used for the cases tested in Figure 13. All cases, coupled and uncoupled, showed at least qualitatively accurate results for the maximum flow rate (Figure 13 left). However, the separate domain coupling cases very inaccurately predicted the maximum pressure drop (Figure 13 right) for larger time steps. In general, the domain overlapping method produced more qualitatively accurate response functions for larger timesteps.

## 5. CONCLUSION AND FUTURE WORK

In this paper, the methods of separate domain coupling and overlapping domain coupling are compared, using an open loop with an abrupt depressurization and a pump driven closed loop simulation as test

cases. The consistency, stability, and convergence characteristics of the methods are compared with the objective of identifying strengths and weaknesses.

Results from overlapping domain cases showed more favorable convergence and stability behavior, primarily due to the system code TRACE performing system wide pressure and flow balances. Splitting the geometry for a separate domain case significantly changes the mathematical structure of the flow loop from the view point of the system code; however its implementation is significantly easier than domain overlapping methods.

Primary ongoing work with the Janus coupling tool is aimed at the extension of the domain overlapping coupling method to transient cases involving the 3D TRACE VESSEL component, with the intention of allowing for coupled simulations of lower plena and general multi-dimensional mixing phenomena inherent to NPPs.

## 6. ACKNOWLEDGMENTS

This work was supported through a DOE NEUP fellowship and the US NRC grant No. NRC-HQ-12-G-04-0083.

## REFERENCES

- [1] U. S. Nuclear Regulatory Commission, *TRACE V5.0 Theory Manual*, 2010.
- [2] INL, "RELAP5-3D Code Manuals Revision 2.3," Idaho National Lab, Idaho Falls, ID, 2005.
- [3] D. Tenchine, R. Baviere, P. Bazin, F. Ducros, G. Geffraye, D. Kadri, F. Perdu, D. Pialla, B. Rameau and N. Tauveron, "Status of CATHARE code for sodium cooled fast reactors," *Nuclear Engineering and Design*, vol. 245, pp. 140-152, 2012.
- [4] G. Lerchel and H. Austregesilo, "ATHLET mod 2.1 Cycle A, User's Manual GRS-p1/Vol1, Rev.4," GRS, Germany, 2006.
- [5] T. Höhne, S. Kliem, U. Rohde and F.-P. Weiss, "Boron Dilution Transients During Natural Circulation Flow in PWR-Experiments and CFD Simulations," *Nuclear Engineering and Design*, vol. 238, pp. 1987-1995, 2008.
- [6] J. H. Jeong and B.-S. Han, "Coolant Flow Field in a Real Geometry of PWR Downcomer and Lower Plenum," *Annals of Nuclear Energy*, vol. 35, pp. 610-619, 2008.
- [7] T.-S. Kwon, C.-R. Choi and C.-H. Song, "Three-Dimensional Analysis of Flow Characteristics on the Reactor Vessel Downcomer During the Late Reflood Phase of a Postulated LBLOCA," *Nuclear Engineering and Design*, vol. 226, pp. 255-265, 2003.
- [8] D. L. Aumiller, E. T. Tomlinson and R. C. Bauer, "A Coupled RELAP5-3D/CFD Methodology with a Proof-of-Principle Calculation," *Nuclear Engineering and Design*, vol. 205, pp. 83-90, 2001.
- [9] H. Gibeling and J. Mahaffy, "Benchmarking Simulations with CFD to 1-D Coupling," Penn State University, Applied Research Laboratory, 2002.
- [10] N. Anderson, Y. Hassan and R. Schultz, "Analysis of the hot gas flow in the outlet plenum of the very high temperature reactor using coupled RELAP5-3D system code and a CFD code," *Nuclear Engineering and Design*, vol. 238, pp. 274-279, 2008.
- [11] D. Bertolotto, A. Manera, S. Frey, H.-M. Prasser and R. Chawla, "Single-phase mixing studies by means of a directly coupled CFD/system-code tool," *Annals of Nuclear Energy*, vol. 36, pp. 310-316, 2009.
- [12] A. Papukchiev, G. Lerchl, C. Waata and T. Frank, "Extension of the Simulation Capabilities of the 1D System Code ATHLET by Coupling with the 3D CFD Software Package ANSYS CFX," in *Proc.*

*The 13th International Topical Meeting on Nuclear Reactor Thermal Hydraulics (NURETH-13)*, Kanazawa City, Ishikawa Prefecture, Japan.

- [13] T. Watanabe, Y. Anoda and M. Takano, "System-CFD coupled simulations of flow instability in steam generator U tubes," *Annals of Nuclear Energy*, vol. 70, pp. 141-146, 2014.
- [14] W. Li, X. Wu, D. Zhang, G. Su, W. Tian and S. Qiu, "Preliminary study of coupling CFD code FLUENT and system code RELAP5," *Annals of Nuclear Energy*, vol. 73, pp. 96-107, 2014.
- [15] T. H. Fanning and J. W. Thomas, "Advances in Coupled Safety Modeling Using Systems Analysis and High-Fidelity Methods," ANL-GENIV-134, 2010.
- [16] D. Pialla, D. Tenchine, S. Li, P. Gauthe, A. Vasile, R. Baviere, N. Tauveron, F. Perdu, L. Maas, F. Cocheme, K. Huber and X. Cheng, "Overview of the system alone and system/CFD coupled calculations of the PHENIX Natural Circulation Test within the THINGS project," *Nuclear Engineering and Design*, vol. ARTICLE IN PRESS, 2015.
- [17] F. Perdu and S. Vandroux, "System/CFD Coupling For Reactor Transient Analysis. An Application To The Gas Fast Reactor With CATHARE And TRIO\_U," in *Proceedings of ICAPP '08*, Anaheim, CA, USA, 2008.
- [18] R. Bavière, N. Tauveron, F. Perdu, E. Garrè and S. Li, "A first system/CFD coupled simulation of a complete nuclear reactor transient using CATHARE2 and TRIO\_U. Preliminary validation on the Phénix Reactor Natural Circulation Test," *Nuclear Engineering and Design*, vol. 277, pp. 124-137, 2014.
- [19] A. Papukchiev, M. Jeltsov, K. Kööp, P. Kudinov and G. Lerchl, "Comparison of different coupling CFD-STH approaches for pre-test analysis of TALL-3D experiment," *Nuclear Engineering and Design*, vol. ARTICLE IN PRESS, 2014.
- [20] G. Bandini, M. Polidori, A. Gerschenfeld, D. Pialla, S. Li, W. M. Ma, P. Kudinov, M. Jeltsov, K. Kööp, K. Huber, X. Cheng, C. Bruzzese, A. G. Class, D. P. Prill, A. Papukchiev, C. Geffray, R. Macian-Juan and L. Maas, "Assessment of Systems Codes and their Coupling with CFD Codes in Thermal-Hydraulic Applications to Innovative Reactors," *Nuclear Engineering and Design*, vol. 281, pp. 22-38, 2015.
- [21] T. L. Bergman, A. S. Lavine, F. P. Incropera and D. P. Dewitt, *Fundamentals of Heat and Mass Transfer: Seventh Edition*, John Wiley & Sons, Inc., 2011.
- [22] F. Cadinu and P. Kudinov, "Development of a "Coupling-by-Closure" Approach between CFD and System Thermal-Hydraulic Codes," in *Proc. The 13th International Topical Meeting on Nuclear Reactor Thermal Hydraulics (NURETH-13)*, Kanazawa City, Ishikawa Prefecture, Japan, 2009.
- [23] D. Bertolotto, *Coupling a System Code with Computational Fluid Dynamics for the Simulation of Complex Coolant Reactivity Effects*, École Polytechnique Fédérale de Lausanne, 2011.
- [24] J. H. Mahaffy, "A Stability-Enhancing Two-Step Method for Fluid Flow Calculations," *Journal of Computational Physics*, vol. 46, pp. 329-341, 1982.
- [25] M. Jeltsov, K. Kööp, P. Kudinov and W. Villanueva, "Development of a Domain Overlapping Coupling Methodology for STH/CFD Analysis of Heavy Liquid Metal Thermal-Hydraulics," in *Proc. The 15th International Topical Meeting on Nuclear Reactor Thermal Hydraulics (NURETH-15)*, Pisa, Italy, 2013.
- [26] CD-Adapco, *STAR-CCM+ v8.02 Manual*, 2013.
- [27] T. H. Fanning and J. W. Thomas, "Integration of CFD into Systems Analysis Codes for Modeling Thermal Stratification During SFR Transients," in *Proc. The 14th International Topical meeting on Nuclear Reactor Thermalhydraulics, NURETH-14*, Toronto, Ontario, Canada, 2011.